Rapid Identification by Surface-Enhanced Raman Spectroscopy of Cancer Cells at Low Concentrations Flowing in a Microfluidic Channel

Alessia Pallaoro,[†] Mehran R. Hoonejani,[‡] Gary B. Braun,[§] Carl D. Meinhart,[*,‡] and Martin Moskovits[*,†]

[†]Department of Chemistry and Biochemistry and [‡]Department of Mechanical Engineering, University of California, Santa Barbara, California 93106, United States and [§]Cancer Research Center, Sanford-Burnham Medical Research Institute, 10901 N. Torrey Pines Road, La Jolla, California 92037, United States

ABSTRACT Reliable identification and collection of cells from bodily fluids is of growing interest for monitoring patient response to therapy and for early detection of disease or its recurrence. We describe a detection platform that combines microfluidics with surface-enhanced Raman spectroscopy (SERS) for the identification of individual mammalian cells continuously flowing in a microfluidics channel. A mixture of cancerous and noncancerous prostate cells was incubated with SERS biotags (SBTs) developed and synthesized by us, then injected into a flow-focused microfluidic channel, which forces the cells into a single file. The spectrally rich SBTs are based on a silver nanoparticle dimer core labeled with a Raman-active small reporter molecule paired with an affinity biomolecule, providing a unique barcode whose presence in a composite SERS spectrum can be deconvoluted. Individual cancer cells passing through the focused laser beam were correctly identified among a proportionally larger number of other cells by their Raman signatures. We examine two deconvolution strategies: principal component analysis and classical least-squares. The deconvolution strategies are used to unmix the overall spectrum to determine the relative contributions between two SBT barcodes, where one SBT barcode indicates neuropilin-1 overexpression, while a second SBT barcode is more universal and indicates unspecific binding to a cell's membrane. Highly reliable results were obtained for all of the cell mixture ratios tested, the lowest being 1 in 100 cells.

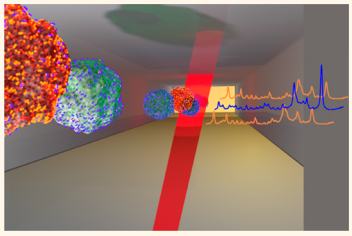

KEYWORDS: SERS · microfluidics · cancer diagnostics · multiplexed · chemometrics

The rapid identification of cancer cells or pathogens in body fluids is a challenging enterprise that is important in both the clinical and research settings. For example, timely identification of certain bacterial strains in blood could modify the choice of treatment and boost survivability from sepsis.[1,2] With cancer, the presence of circulating tumor cells (CTCs) in blood has been correlated with disease outcome and patient survival for a number of specific cancers;[3] however, the routine identification of CTCs as disease markers, for example, in blood is not yet widespread,[4] partly due to the biological complexity of cancer,[5] which is exacerbated by the variability of the reported data[6] and lack of standardized definitions.[7] The major challenges in rapid cell and pathogen detection arise from the need for a sensitive, reliable, automated high-throughput method[8] for identifying subgroups of closely related cells, *e.g.*, CTCs from tumors escaping the epithelial phenotype.[9] Detection of parameters such as stemness markers[1,2,10] or other unique cell- and species-specific antigens or receptors[3,11−14] is of primary interest in assay development in addition to the more traditional epithelial markers.

Cancer cell and pathogen diagnostics entail capturing, analyzing, and, in some cases, propagating a small number of cells, procedures that would benefit from advancements in manipulating small volumes and individual cells. A variety of techniques have been developed for manipulating and analyzing cells using various approaches including immunocapture with antigen-based fluorescence detection,[4,15−18] label-free biomechanical separation,[5,19] and fluorescence-based cytometry in microfluidic channels.[6,20] The improvement of modular, on-chip, microfluidics systems combined with rapid spectroscopic detection would greatly advance continuous single-cell analysis.[7,21]

* Address correspondence to moskovits@chem.ucsb.edu, meinhart@engineering.ucsb.edu.

Received for review February 2, 2015 and accepted March 17, 2015.

Published online March 17, 2015
10.1021/acsnano.5b00750

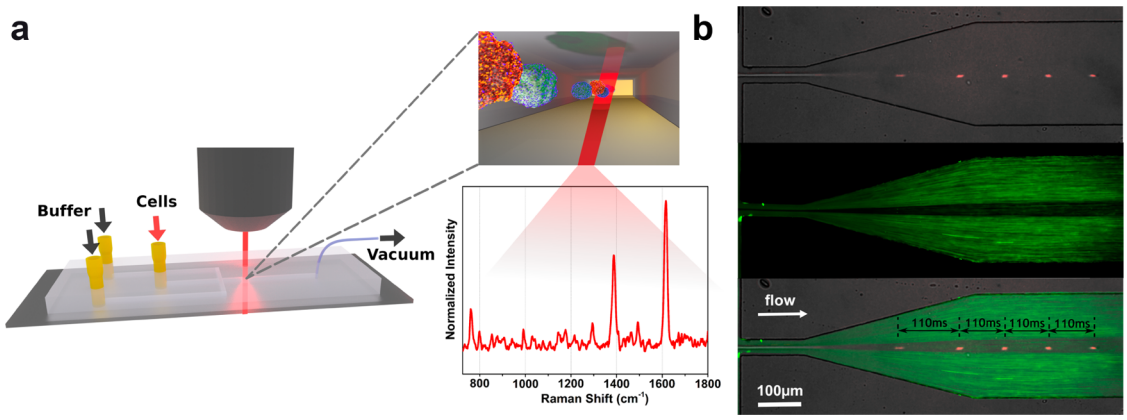

Figure 1. Graphical depiction of device layout and flow dynamics. (A) Schematic of setup and concept. Cells, prelabeled with a cocktail of cancer-specific (NRP) and control (UC) SBTs (the latter binding both cell types), are injected into the device, where they are flow-focused before passing through the Raman laser. (B) Simultaneous bright-field and epifluorescence (Cy3 channel, colorized orange) image of a single cell in the channel as a function of time illustrating the efficacy of flow focusing (top). Epifluorescence image (FITC channel, colorized green) of 200 nm polymer beads separately injected into the buffer channels, to highlight the sheath flow (center). Montage merging the two former images (bottom), showing the overall flow dynamics in the device. A video shows cells flowing in the device in single file (Video S1) is available.

Label-free Raman spectroscopy can differentiate cancer from normal cells[8,22−25] or bacterial strains[26] *via* subtle compositional differences in amino acid, nucleic acid, or lipids, which generate weak, broadly overlapping but, in certain cases, decipherable spectra. Surface-enhanced Raman spectroscopy (SERS) is a powerful method for cancer cell detection because of its very much higher intensity (compared to normal Raman) and narrower spectral bands relative to fluorescence,[27] which enables multiple marker recognition. SERS has been used for cancer biomarker[28−30] and pathogen[12,31−33] detection and cell and tissue imaging,[34−38] but to date, only a few examples of SERS cytometry[39,40] have been reported, none using SERS tags in microfluidics.

SERS signals arise from molecules residing in the clefts or interstices in metal nanostructures.[41,42] SERS fingerprinting has been used to identify and quantitatively measure concentrations of analytes[43,44] and has had notable success in a microfluidics context.[45−47] Recent reports exploiting SERS for CTC[48,49] and pathogen detection have shown promise in recognizing cells by either the intensity of a bound SERS reporter probe or the normal Raman features of cells being sufficiently surface-enhanced through contact with metal nanostructures.[50] While these advances are significant, additional biological insight is expected from analysis of single cell receptor expression patterns beyond the simple cell count or positive/negative type of response. We have previously reported the synthesis of bright and stable SERS-based tags (SBTs, SERS biotags) that are stable in biological conditions and can bind mammalian cells[43,51,52] and have demonstrated multiplexed cell identification based on surface marker expression through point-by-point microscopic analysis of cells deposited on a glass surface.[51]

Here, we describe a microfluidic chip-based cell identification system that uses SERS to detect live mammalian cells labeled with mixtures of two spectroscopically distinguishable SBTs that target distinct cell epitopes. Cells forced by hydrodynamic flow focusing into a single file at the center of the microfluidic channel cross a focused laser beam at the interrogation region, exciting the cell-bound SBTs. SERS identification of cells takes place "on the fly" by measuring the relative signal from a cancer-specific marker *versus* a cell-identifying universal control marker. Two analytical methods are employed to categorize a cell as cancerous or normal: a chemometric algorithm developed by us based on principal component analysis (PCA) of the cell populations and a least-squares deconvolution of SBT spectra into known "pure" components, from which the receptor ratio was calculated. In our approach, we exploit the high emission cross-section of SERS from SBTs and leverage a new chemometric approach for categorizing spectra, thus avoiding sensitivity to focus and enabling reliable single-cell identification in microfluidics (Figure 1).

RESULTS AND DISCUSSION

SBTs were assembled using in-house-synthesized citrate-protected silver nanoparticle monomers (~45 nm diameter) that are controllably aggregated into small clusters using phosphate and hexamethylenediamine and encapsulated in polyvinlypyrrolidone for stability (Figure S1) (see Materials and Methods for details). A modified bovine serum albumin imparts further stability and limits nonspecific cellular interactions, while offering a handle for conjugation with cell-targeting moieties, through the thiol-reactive SPDP (succinimidyl 3-(2-pyridyldithio)propionate) group.[51] Neuropilin-1 (NRP-1), a receptor that is overexpressed on the membrane of cells in several cancers,[53] was

chosen as a cancer-specific biomarker for NRP-SBTs, while the HIV-derived cell-penetrating peptide TAT was used as universal control (UC-SBTs). We used NRP-1-overexpressing prostate cancer cells (PPC-1) and normal RWPE-1 cells to demonstrate the specificity of detection. Cells were harvested, mixed with the SBT cocktail, and incubated for 60 min at room temperature on a tube rotator. After washing excess unbound SBTs from the cells by centrifugation, the cells were either mixed at specific cancer/normal ratios or used pure as references and individually injected into the flow-focusing PDMS-based microfluidic device (Figure 1).

The device was designed with one inlet for sheath buffer, one inlet for sample, and an outlet (Figure 1A). The flow rate ratio between sheath and cell flow was regulated by the geometry of the inlet and outlet channels.[54] A SERS spectrum was acquired for each cell that passed through the laser. A typical run took approximately 8 min; however the device could be operated continuously without clogging or saturating for several hours, in contrast to microfluidic-capture technologies, where cells are captured on surfaces or other features in the device. The flow rates and other engineered features of the device were chosen so that each cell would spend approximately 5−8 ms in the laser beam.

SERS Analytical Strategy. Two strategies were used for the analysis of single cell flow data: (i) principal component analysis and (ii) classic least-squares (CLS), using a custom Matlab algorithm, to compare the relative performance of each model for cancer cell identification.

The SERS-microfluidics system was initially characterized by flowing and analyzing reference samples consisting of either pure PPC-1 (cancer) or pure RWPE-1 (noncancerous) SBT-labeled cells. PPC-1 cells bind to both NRP-SBTs and UC-SBTs, whereas RWPE-1 binds predominantly to the UC-SBTs, with very low, mainly nonspecific interaction with NRP-SBTs. Spectra were collected every 100−150 ms, for a total of ~1700 full spectra (events) per run. To reduce the size of the collected data, we first applied a "gating" PCA algorithm (gPCA) (Figure 2) to remove the spectra that contained only those peaks associated with PDMS, the polymeric material from which the flow device was fabricated. This gating left only the spectra that included cell-related spectroscopic signals in convolution with the PDMS background. In this step, the spectra were preprocessed by baseline subtraction, normalization by the total band area in the 280−1800 cm^{-1} wavenumber range, and mean centering, before gPCA analysis was carried out. No smoothing was applied to the spectra during preprocessing. The gPCA model was generated using PLS Toolbox (Eigenvector Research, Inc., Wenatchee, WA, USA), and one principal component (gPC1) was found,

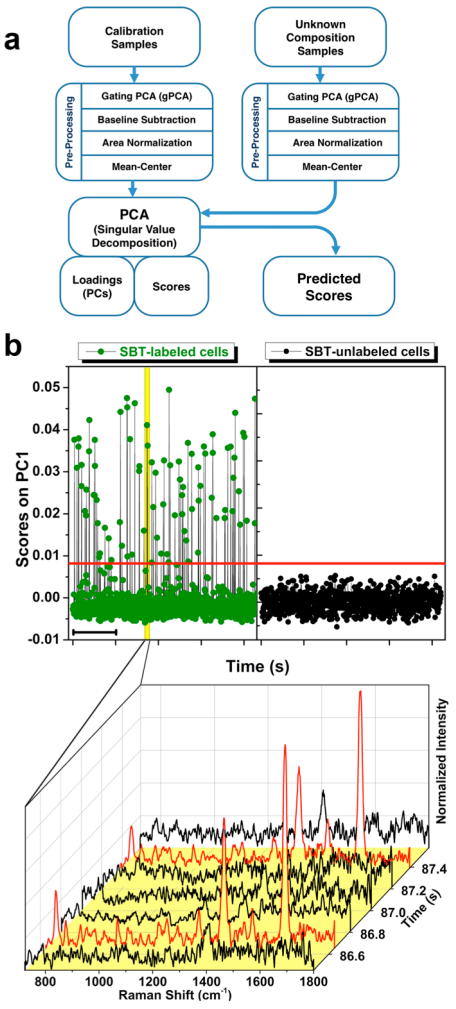

Figure 2. Analysis of spectral data by PCA to classify cells as either cancerous or normal. (A) Flowchart summarizing the sequence of steps in our chemometric analysis by PCA. (B) The upper panel shows the gPC1 scores for spectra from two data sets (mix of SBT-labeled cancerous and normal cells, green dots; mix of CellTracker orange labeled cancer cells and unlabeled noncancerous cells, black dots), returned by the gating PCA model generated to gate spectra showing peaks associated with SBTs (high scores on gPC1) over those showing only spectral contributions associated with PDMS (gPC1 scores around 0). A gating threshold (red horizontal line) was chosen based on the upper 95% confidence limit of the gPC1 scores and was adjusted manually depending on the signal/noise of the spectra around that value. The lower panel shows a series of spectra collected over approximately 2 s, corresponding to the time fraction highlighted in the yellow box in the upper panel. Spectra associated with events below the gating threshold, showing only PDMS-related bands, are depicted in black, and spectra with SBTs-associated peaks and gPC1 scores above the gating threshold are shown in red. Spectra were smoothed for clarity of presentation, but no smoothing was used for the analysis.

which contained the spectral features characteristic of SBTs, in addition to those associated with PDMS (Figure S2). Accordingly, gPC1 was taken to be a reliable criterion for gating cell events (Figure 2B, upper panel). Each data point in the upper panel of Figure 2B corresponds to a Raman spectrum. The lower panel shows a magnified view of the typical spectra (after

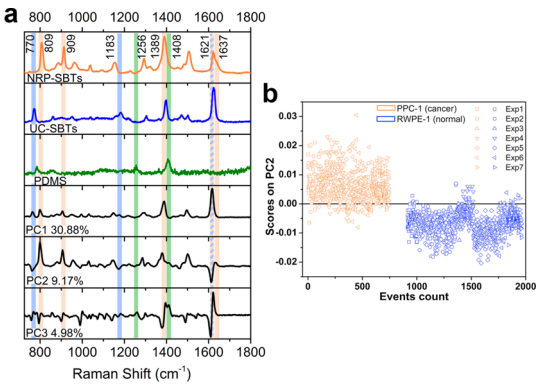

Figure 3. Summary of results returned by principal component analysis of the reference data set consisting of pure cancer and noncancerous cells. (A) Reference spectra of SBTs and PDMS (upper three plots) and principal components (PCs, lower three plots). Color coding identifies spectral bands unique to either SBTs or PDMS: UC-SBTs (blue), NRP-SBTs (orange), PDMS bands (green). The alternating blue/orange highlight identifies one band that in UC-SBTs is dominant and narrow (fwhm 16.5 cm^{-1}), but in NRP-SBTs is broad (fwhm 25.4 cm^{-1}), showing a shoulder at 1637 cm^{-1} (orange marker). (B) PC2 scores obtained from selected reference data sets of pure PPC-1 (mostly positive scores) and pure RWPE-1 cells (mostly negative scores).

preprocessing) acquired over approximately 2 s. The black spectra show only Raman peaks associated with PDMS, which scored gPC1 values below the gating threshold (red line) corresponding to the upper 95% confidence interval of the model. The spectra in red, instead, scored gPC1 values above the gating threshold, indicating that they contained Raman bands associated with either NRP-SBTs or UC-SBTs (Figure 2B). These reduced data sets were analyzed by PCA and CLS.

Principal Component Analysis of Pure Cell Populations. A PCA model (generated using the PLS Toolbox) was constructed using the reference spectra of pure normal and cancer cells as calibration sets from which the principal components (PCs) were determined. Three components (PC1, PC2, and PC3) were found to describe approximately 45% of the overall variability of the data (Figure 3A). The remaining 55% was found to be associated with residuals mainly generated by noise (Figure S3). A comparison between the principal components and reference Raman spectra of PDMS, and SERS spectra of NRP-SBTs (carrying the Raman reporter thionin) and UC-SBTs (carrying the Raman reporter methylene blue) (Figure 3A), shows that PC1 is primarily composed of positive peaks identifying bands of both NRP-SBTs and UC-SBTs, PC3 consists mainly of spectral features of PDMS, and PC2 consists of negative peaks corresponding to UC-SBTs bands at 1183 and 770 cm^{-1} and positive peaks correspond to NRP-SBTs bands (1389, 909, and 809 cm^{-1}). PC2 also shows a negative peak at 1621 cm^{-1} and a positive peak at 1637 cm^{-1} (Figure 3A). The former (1621 cm^{-1}) is a feature present in the spectra of both the UC-SBT and NRP-SBT, while the latter (1637 cm^{-1}) coincides with a shoulder in the spectrum of NRP-SBT. Clearly PC2 is the component that discriminates confidently and strikingly between cancerous and normal cells. Quantitatively, 95% of the cancerous cells showed positive values of PC2 scores, while 95% of the noncancerous cells produced negative PC2 scores. PC2 scores determined from experiments in which pure cell population samples were flowed are shown in Figure 3B. A full data set that includes experiments run on different days and under different experimental conditions is shown in Figure S4.

Classical Least-Squares Analysis of Pure Cell Populations. The SERS results were also analyzed by CLS (Figure S4), which assumes that a given composite spectrum is a linear combination of the SERS spectra of the individual tags, with the coefficients indicating the relative quantitative contribution of a given individual tag to the composite. The coefficients returned by the CLS analysis were used to calculate the ratio NRP/UC for the reference samples. The CLS model was constructed based on a calibration set consisting of the composite SERS spectra obtained from five mixtures of NRP-SBTs and UC-SBTs at known relative concentrations together with the Raman spectrum of PDMS. Pure components were calculated using this calibration set and the known contributions of each tag. The NRP/UC ratios for any spectrum with unknown NRP-SBT and UC-SBT concentration were then calculated based on the contribution of each SBT predicted by the CLS model. All the spectra were preprocessed prior to CLS analysis (Figure S5), as described above.

Figure 4A summarizes graphically the statistics of the data analyzed by CLS. For the RWPE-1 (normal) cells, 95% show NRP/UC ratios below 0.72, and 95% of PPC-1 cells (cancer) have NRP/UC > 0.71, in good agreement with our previous report.[51] Statistical analysis (Mann−Whitney test, $N = 686$ for cancer cells and $N = 1013$ for normal cells) confirms the two cell populations to be significantly different at the 0.001 level. Note that these data were each collected in at least three sets of experiments, using stocks of SBTs synthesized from scratch on several occasions (indicating the reproducibility of the SBTs) and cell stocks separately thawed from a frozen repository, thereby demonstrating the reproducibility of the procedure across the biological variability spectrum. Cells that were not incubated with SBTs were not detectable by SERS, as shown in Figure 2B, where all the recorded spectra show approximately zero gPC1 scores, indicating that only PDMS bands were present in the SERS spectra.

SERS-Microfluidic Chip Analysis of Cancer and Normal Cells Mixed Together. To determine the SERS-microfluidic chip's ability to detect cancer cells in low concentration against a background of other cells, samples were prepared that comprised mixtures of normal and cancer cells with varying ratios. Samples ranging from

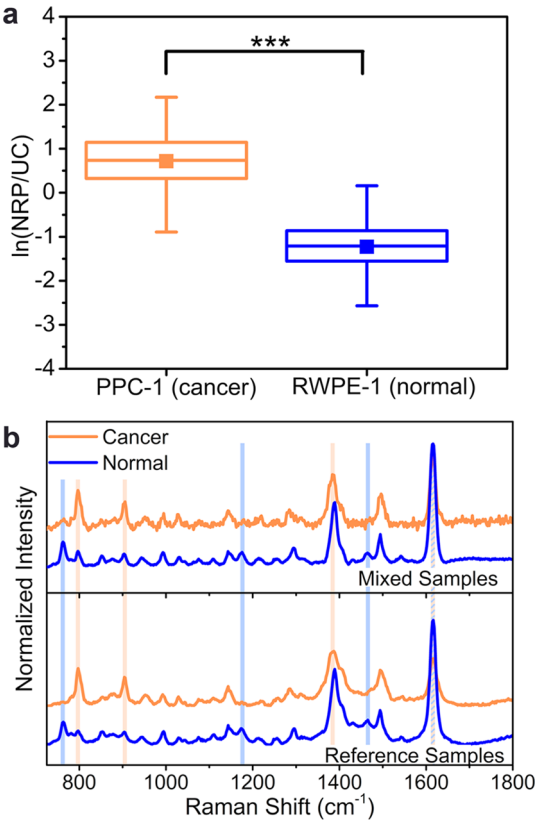

Figure 4. Analysis of SERS data by CLS. (A) Box plots of reference data for normal (RWPE-1) and cancer (PPC-1) cells showing the ln(NRP/UC) as calculated from the CLS analysis. The boxes are well separated along the ln(NRP/UC) axis, confirming that the ratiometric SERS is a robust discriminant for cancer cell detection. The two populations are statistically different, Mann−Whitney test, $p < 0.001$. (B) Average SERS spectra of RWPE-1 and PPC-1 cells from reference data compared to the average spectra of cells classified as either cancer or normal by CLS from a sample containing a mixture of the two cell types with 5% cancer cells. Orange and blue highlighting indicates bands predominant in NRP-SBTs and UC-SBTs, respectively.

2% to 50% cancer cells among normal cells (all incubated with SBTs) were injected into the devices, and SERS signatures from SBT-labeled cells were recorded using the same protocol as was used in the calibration runs.

Both PCA and CLS were used to analyze the data. Cancer cell identification was based on the SBT statistics determined in the reference set, which for PCA was a PC2 threshold score greater than zero (Figure 3B) and for CLS, a NRP/UC ratio greater than 1.14, a value below which 99% of normal cells lie (Table S1). Cell events above threshold were classified as cancerous; all others as noncancerous. Figure 4B shows the average SERS spectra of reference RWPE-1 (blue) and PPC-1 (orange) cells, compared with the average SERS spectra from a 5% cancerous/95% noncancerous cell mixture, which was analyzed by CLS. The spectra of the cells assigned to each group by CLS (and by PCA, not shown) were in good agreement with the reference spectra, having all the major identifying peaks (highlighted by the orange and blue markers). Cells identified as cancerous did not have as prominent UC-SBTs bands (770 and 1180 cm^{-1}) as normal cells. Cancer cells also showed a weaker 1620 cm^{-1} band intensity than normal cells, which ideally should bind only UC-SBTs, and the band was broader, similar to the cancer cell reference spectrum.

Figure 5 summarizes the results of the spectral analysis of the cell mixtures. Cells above the respective PCA and CLS thresholds (as determined by the methodology described above using pure cancerous and normal cell populations) were counted as cancerous, and their percentage of the total number of cells detected was plotted against the nominal percentage of cancer cells introduced in the sample. The results returned by the computations are in good agreement (Figure 5A) with the as-prepared (nominal) sample composition, with a linear relationship from 0% to 100% cancer cells ($r^2 = 0.999$ for CLS and $r^2 = 0.995$ for PCA), indicating excellent accuracy of both models for the cell classification. On the basis of the results in Figure 5A, we could reliably detect cancer cells down to 2%, by both CLS and PCA. Detecting such a low percentage of cancer cells would be challenging for microscopic mapping without enrichment of the sample. The results from PCA and CLS computations were also compared to each other. Figure 5B shows good agreement between detected cancer cell percentages as determined by the two methods. At very low cancer cell composition (0−5%), ratiometric analysis by CLS shows superior performance at detecting the proper number of cancer cells in an excess of normal, SBT-labeled cells, compared to PCA.

For CLS ratiometric analysis (Figure 5), the minimum percentage detectable (limit of detection) is influenced by the threshold value that identifies cancer cells as those events residing above threshold (Figure 4B). This value was chosen so that less than 1% of normal cells were above threshold. In order to reduce the limit of detection for rare cancer cells, it would be critical (for PCA or CLS) that the separation between normal and cancer cells along the detection coordinate be maximized. To detect 1% cancer cells within a mixture, a more conservative threshold could be established with much fewer normal cells above it (*e.g.*, 0.1% of normal cells above). To reduce further the probability of normal cells registering above threshold, refinements to the specificity of the SBT coating or additional SBTs (specifically tagging unique receptors) can be introduced, opening up new detection coordinates.

It is worth noting that although the above detection limit may seem too high for applications such as CTC detection from whole blood, it refers to the identification of a specific population of SBT-labeled cells that give a SERS signal; a multitude of SERS-inactive unlabeled cells (Figure 2B), *e.g.*, blood cells, may be tolerated without degrading the sensitivity. This SBT

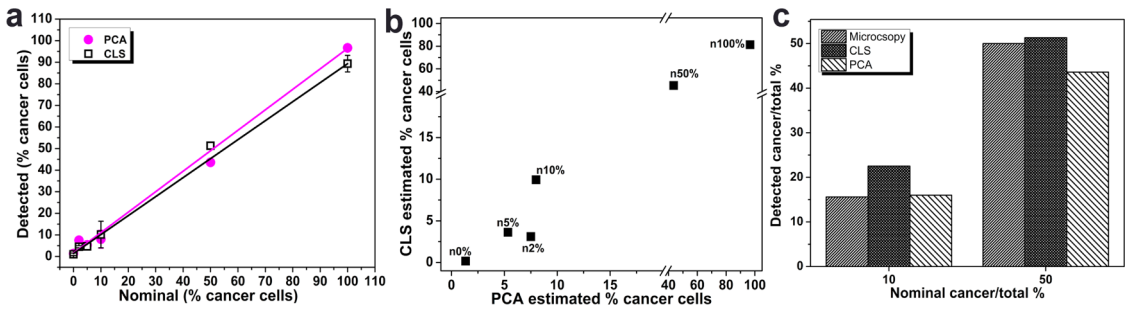

Figure 5. Comparison of results from PCA and CLS analysis at low cancer cell concentration. (A) The percentage of cancer cells detected by PCA (magenta, solid symbols) and CLS (black, open symbols) is plotted against the nominal percent (indicating the composition loaded in the device reservoir). Error bars indicate ± SEM (standard error of the mean). (B) PCA and CLS detection performance across a range of sample compositions. Labels for each data point indicate the nominal cancer cell percentage of each sample. (C) Bar graph comparing cancer cell counts by microscopy, PCA, and CLS. Cancer cells were labeled with CTO, prior to incubation with SBTs, and mixed with RWPE-1 cells. Before injecting the sample into the device an aliquot was placed on a microscope slide and fluorescent cells were counted, comparing the results with PCA and CLS and against the nominal value.

labeling strategy could be employed along with other cell enrichment methods for processing increased volumes of whole blood for CTC detection.

PCA (Figures 3 and 5) was shown to be a successful strategy for distinguishing cancer cells from their noncancerous counterparts, in a set of spectra derived from multiple cells interrogated using microfluidics, while significantly increasing the throughput over microscopic imaging.[51] In scenarios where pure cell populations are not known *a priori*, PCA appears to be the strategy of choice for classification, while CLS yields more comprehensive biological detail regarding the quantitative levels of receptor expression. In some instances, given the complex relationships among CTC cells and their subgroups (*e.g.*, epithelial, mesenchymal, overexpressing cancer biomarkers) that differ subtly from one another, cells may need to be labeled with a larger number of tags for their proper differentiation. Chemometric PCA and CLS analyses can be scaled up to deal with such more complex analyses, although the implementation becomes progressively complex as the number of tags increases. Under such circumstances CLS, which we showed has great resilience to variations in flow dynamics and laser focal-plane fluctuations, could augment PCA through pairwise receptor overexpression analysis designed to highlight biological patterns and diversity.

Validation of PCA and CLS Analysis of Mixed Cell Samples. In selected experiments, in addition to SBT-labeling, cancer cells were fluorescently stained with CTO (CellTracker orange) and mixed with normal cells without fluorescent dye at either 50% or 10% of the total for microscopic characterization. The dye does not have a SERS signature (Figure 2B, black dots). Fluorescence microscopy was used to determine the composition of the samples prior to injection (Figure S6) and during flow (rather than relying on the accuracy of the nominal composition). Prior to injection, cells were placed on glass slides and the number of fluorescently labeled cells counted. An average of 50 images per sample (~480 cells/sample) were analyzed. The fraction of cells that registered positive by fluorescence agreed well with the nominal value, validating the sample preparation protocol (Figure 5C). Cell counting by microscopy also validated the CLS2 and PCA analysis, indicating the level of confidence with which those algorithms are able to identify cells.

CONCLUSION

An integrated microfluidic SERS system is described that identifies and counts cancer cells from a population of cells flowing through a microfluidic channel. The resulting signals are analyzed by deconvolving SERS signals originating from two affinity labels excited by a single laser. The two cell-targeting SBTs were selected so that one binds cancer cells specifically, while the other binds nonspecifically and functions as a non-cell-specific control. The reporter molecules each contributed a unique Raman spectrum. We adapted two algorithms for distinguishing cancerous cells from normal cells: (i) principal component analysis and (ii) classical least-squares. The relative merits of the two models are compared for identifying low-concentration cancerous cells from a population of noncancerous cells. PCA has the advantage that it does not require reference spectra, whereas the CLS can confidently—and more importantly quantitatively—report the relative contribution of each targeted receptor species to the overall spectrum by deconvolution. The spectroscopic richness of the Raman bands of the reporter molecules residing on the two SBTs was fundamental for the successful categorization of cells, down to one cancer cell from a population of 100 noncancerous cells, while being interrogated by the laser beam for 20 ms.

The approach is shown to be highly insensitive to such parameters as the small batch-to-batch variability in the properties of the SBTs, flow rate, and integration times. The approach provides one-step cell labeling,

continuous cell analysis, a disposable low-cost device, and nondestructive tumor cell identification, and offers a clear path to multiplexed receptor expression analysis at the single-cell level.

MATERIALS AND METHODS

SERS Biotag Synthesis and Assembly. SBTs were synthesized as described in the SI. The appropriate Raman reporter and cell targeting peptide (methylene blue and FAM-cys-TAT for UC-SBTs; thionin and FAM-cys-RPARPAR for NRP-SBTs) were attached to the SBTs.

Cell Culture. PPC-1 cells were a generous gift from Erkki Rouslahti's group (Sanford-Burnham Medical Research Institute, UC Santa Barbara). RWPE-1 cells were from ATCC. Cells were cultured (see SI), harvested using a nonenzymatic cell dissociation buffer (Invitrogen #13151-014), washed by centrifugation, and resuspended in the appropriate volume of DMEM + 10% FBS in order to obtain a concentration of 1.0×10^6 cells/mL. SBTs were then added (with UC *versus* NRP ratio of 1:1 v/v) and incubated for 60 min at room temperature on a tube rotator to guarantee mixing and avoid cell settling. Excess unbound SBTs in the supernatant were removed after centrifugation, and samples for injection into the devices in measurement buffer (SI) were supplemented with 19% OptiPrep (Sigma).

For fluorescence microscopy analysis, PPC-1 cells were stained with CellTracker orange (Life Technologies) prior to harvesting. Cells were imaged using an Olympus BX41 microscope.

Device Fabrication. The microfluidic device was designed based on ref 54. The geometry of the inlet and outlet channels determined the flow rate ratio between the sheath and sample flows. The devices were made of PDMS (Sylgard 184) using an SU-8 mold and standard soft lithography techniques and sandwiched between two microscopy glass slides (SI). Holes were drilled through the glass to correspond to the channel holes, and pipet tips were inserted to serve as reservoirs and connection ports to the tubing. The flow was actuated by a diaphragm vacuum pump (Gast Manufacturing Corporation) connected to the outlet of the device. The channel dimensions were 50 μm wide by 40 μm deep, and the sample flow was focused down to 7 μm after the junction. The wide interrogation section of the outlet channel was 350 μm wide. The centerline fluid velocity in the interrogation region was designed to be 2 mm/s. Cell-containing samples were injected into the middle channel, and buffer was used for the sheath flow in the side channels.

SERS Measurements. The SERS measurements were carried out on a Horiba Jobin-Yvon LabRAM Aramis spectrometer, equipped with a 633 nm laser for excitation. The laser was focused through a 10× objective (11 mW power at sample) with integration time set to 20 ms. Points were acquired every 100−150 ms for approximately 8 min for each run. The slit was set to 250 μm and the hole to 600 μm, and a 600 gr/mm grating was used.

Data Analysis. A custom Matlab (Mathworks, Inc., Natick, MA, USA) algorithm was developed to preprocess and analyze the spectral data (see SI). "Gating" PCA data set size reduction was performed using the PLS Toolbox (Eigenvector Research, Inc.) on all the data, in order to remove all the spectra showing only peaks attributed to PDMS. The raw spectra (from the reduced data set) were baseline subtracted by a weighted least-squares filter, normalized based on the area under the spectrum from 725 to 1800 cm^{-1}, and mean-centered. Data analysis was done with PCA. PCA was performed to categorize the spectra of normal and cancer cells using the PLS Toolbox. The PCA model (see SI) was constructed using the reference spectra of pure normal and cancer cells (calibration set) to find the PCs. The spectra recorded from samples containing cancer and normal cells mixed together were tested by the model to determine their scores on the basis of the PCs found through the calibration set. The scores on PC2 were then used to classify each cell as either cancer or noncancerous. Data analysis was done with classic least-squares. Spectral deconvolution was performed using PLS Toolbox with a classic least-squares model that we trained with a calibration set consisting of five mixtures consisting of NRP-SBTs and UC-SBTs combined at known relative ratios and the Raman spectrum of PDMS (see SI). The CLS determined the ratio of the contribution of each SBT to the cell's spectrum (NRP as a cancer marker and UC as a universal control). The NRP/UC ratios were assumed to be the ratio of the coefficients returned by the CLS model.

Conflict of Interest: The authors declare no competing financial interest.

Supporting Information Available: More detailed methods description, additional figures, and statistical analysis. A video of cells flowing in the device. This material is available free of charge *via* the Internet at http://pubs.acs.org.

Acknowledgment. We thank Prof. Norbert Reich for cell culture facility use and Prof. Stanley Parsons for fluorescence microscope use. This work was supported by the Institute for Collaborative Biotechnologies through grant W911NF-09-0001 from the U.S. Army Research Office. The content of the information does not necessarily reflect the position or the policy of the Government, and no official endorsement should be inferred. Financial support from the University of California Cancer Research Coordinating Committee is also gratefully acknowledged. A.P., M.R.H., G.B.B., C.D.M., and M.M. designed the research; A.P. and M.R.H. collected the data; A.P., M.R.H., and G.B.B. analyzed the data; A.P., C.D.M., and M.M. wrote the manuscript.

REFERENCES AND NOTES

1. Kumar, A.; Ellis, P.; Arabi, Y.; Roberts, D.; Light, B.; Parrillo, J. E.; Dodek, P.; Wood, G.; Kumar, A.; Simon, D.; *et al.* Initiation of Inappropriate Antimicrobial Therapy Results in a Fivefold Reduction of Survival in Human Septic Shock. *Chest* **2009**, *136*, 1237–1248.
2. Daniels, R. Surviving the First Hours in Sepsis: Getting the Basics Right (an Intensivist's Perspective). *J. Antimicrob. Chemother.* **2011**, *66*, ii11–ii23.
3. Miller, M. C.; Doyle, G. V.; Terstappen, L. W. M. M. Significance of Circulating Tumor Cells Detected by the CellSearch System in Patients with Metastatic Breast Colorectal and Prostate Cancer. *J. Oncol.* **2010**, *2010*, 617421–617421.
4. Scher, H. I.; Morris, M. J.; Larson, S.; Heller, G. Validation and Clinical Utility of Prostate Cancer Biomarkers. *Nat. Rev. Clin. Oncol.* **2013**, *10*, 225–234.
5. Joosse, S. A.; Pantel, K. Biologic Challenges in the Detection of Circulating Tumor Cells. *Cancer Res.* **2013**, *73*, 8–11.
6. Krebs, M. G.; Hou, J. M.; Ward, T. H.; Blackhall, F. H.; Dive, C. Circulating Tumour Cells: Their Utility in Cancer Management and Predicting Outcomes. *Ther. Adv. Med. Oncol.* **2010**, *2*, 351–365.
7. Coumans, F. A. W.; Doggen, C. J. M.; Attard, G.; de Bono, J. S.; Terstappen, L. W. M. M. All Circulating EpCAM+ CK+CD45− Objects Predict Overall Survival in Castration-Resistant Prostate Cancer. *Ann. Oncol.* **2010**, *21*, 1851–1857.
8. Yu, M.; Stott, S. L.; Toner, M.; Maheswaran, S.; Haber, D. A. Circulating Tumor Cells: Approaches to Isolation and Characterization. *J. Cell Biol.* **2011**, *192*, 373–382.
9. Barrière, G.; Tartary, M.; Rigaud, M. Epithelial Mesenchymal Transition: A New Insight Into the Detection of Circulating Tumor Cells. *ISRN Oncol.* **2012**, *2012*, 1–6.
10. Kasimir-Bauer, S. S.; Hoffmann, O. O.; Wallwiener, D. D.; Kimmig, R. R.; Fehm, T. T. Expression of Stem Cell and Epithelial-Mesenchymal Transition Markers in Primary

Breast Cancer Patients with Circulating Tumor Cells. *Breast Cancer Res.* **2012**, *14*, R15–R15.
11. Yu, M.; Bardia, A.; Wittner, B. S.; Stott, S. L.; Smas, M. E.; Ting, D. T.; Isakoff, S. J.; Ciciliano, J. C.; Wells, M. N.; Shah, A. M.; *et al*. Circulating Breast Tumor Cells Exhibit Dynamic Changes in Epithelial and Mesenchymal Composition. *Science* **2013**, *339*, 580–584.
12. Stephen, K. E.; Homrighausen, D.; DePalma, G.; Nakatsu, C. H.; Irudayaraj, J. Surface Enhanced Raman Spectroscopy (SERS) for the Discrimination of Arthrobacter Strains Based on Variations in Cell Surface Composition. *Analyst* **2012**, *137*, 4280–4286.
13. Maeng, J.-S.; Kim, N.; Kim, C.-T.; Han, S. R.; Lee, Y. J.; Lee, S.-W.; Lee, M.-H.; Cho, Y.-J. Rapid Detection of Food Pathogens Using RNA Aptamers-Immobilized Slide. *J. Nanosci. Nanotechnol.* **2012**, *12*, 5138–5142.
14. Chang, Y.-C.; Yang, C.-Y.; Sun, R.-L.; Cheng, Y.-F.; Kao, W.-C.; Yang, P.-C. Rapid Single Cell Detection of Staphylococcus Aureus by Aptamer-Conjugated Gold Nanoparticles. *Sci. Rep.* **2013**, *3*, 1863–1863.
15. Stott, S. L.; Hsu, C.-H.; Tsukrov, D. I.; Yu, M.; Miyamoto, D. T.; Waltman, B. A.; Rothenberg, S. M.; Shah, A. M.; Smas, M. E.; Korir, G. K.; *et al*. Isolation of Circulating Tumor Cells Using a Microvortex-Generating Herringbone-Chip. *Proc. Natl. Acad. Sci. U.S.A.* **2010**, *107*, 18392–18397.
16. Gleghorn, J. P.; Pratt, E. D.; Denning, D.; Liu, H.; Bander, N. H.; Tagawa, S. T.; Nanus, D. M.; Giannakakou, P. A.; Kirby, B. J. Capture of Circulating Tumor Cells From Whole Blood of Prostate Cancer Patients Using Geometrically Enhanced Differential Immunocapture (GEDI) and a Prostate-Specific Antibody. *Lab Chip* **2010**, *10*, 27–29.
17. Ozkumur, E.; Shah, A. M.; Ciciliano, J. C.; Emmink, B. L.; Miyamoto, D. T.; Brachtel, E.; Yu, M.; Chen, P. I.; Morgan, B.; Trautwein, J.; *et al*. Inertial Focusing for Tumor Antigen-Dependent and -Independent Sorting of Rare Circulating Tumor Cells. *Sci. Transl. Med.* **2013**, *5*, 179ra47–179ra47.
18. Mikolajczyk, S. D.; Millar, L. S.; Tsinberg, P.; Coutts, S. M.; Zomorrodi, M.; Pham, T.; Bischoff, F. Z.; Pircher, T. J. Detection of EpCAM-Negative and Cytokeratin-Negative Circulating Tumor Cells in Peripheral Blood. *J. Oncol.* **2011**, *2011*, 1–10.
19. Jin, C.; McFaul, S. M.; Duffy, S. P.; Deng, X.; Tavassoli, P.; Black, P. C.; Ma, H. Technologies for Label-Free Separation of Circulating Tumor Cells: From Historical Foundations to Recent Developments. *Lab Chip* **2014**, *14*, 32–44.
20. Fu, A. Y.; Spence, C.; Scherer, A.; Arnold, F. H.; Quake, S. R. A Microfabricated Fluorescence-Activated Cell Sorter. *Nat. Biotechnol.* **1999**, *17*, 1109–1111.
21. Hyun, K.-A.; Jung, H.-I. Advances and Critical Concerns with the Microfluidic Enrichments of Circulating Tumor Cells. *Lab Chip* **2014**, *14*, 45–56.
22. Wang, L. Raman Spectroscopy, a Potential Tool in Diagnosis and Prognosis of Castration-Resistant Prostate Cancer. *J. Biomed. Opt.* **2013**, *18*, 087001–087001.
23. Terentis, A. C.; Fox, S. A.; Friedman, S. J.; Spencer, E. S. Confocal Raman Microspectroscopy Discriminates Live Human Metastatic Melanoma and Skin Fibroblast Cells. *J. Raman Spectrosc.* **2013**, *44*, 1205–1216.
24. Lau, A. Y.; Lee, L. P.; Chan, J. W. An Integrated Optofluidic Platform for Raman-Activated Cell Sorting. *Lab Chip* **2008**, *8*, 1116–1120.
25. Neugebauer, U.; Bocklitz, T.; Clement, J. H.; Krafft, C.; Popp, J. Towards Detection and Identification of Circulating Tumour Cells Using Raman Spectroscopy. *Analyst* **2010**, *135*, 3178–3182.
26. Goeller, L. J.; Riley, M. R. Discrimination of Bacteria and Bacteriophages by Raman Spectroscopy and Surface-Enhanced Raman Spectroscopy. *Appl. Spectrosc.* **2007**, *61*, 679–685.
27. Sabatté, G.; Keir, R.; Lawlor, M.; Black, M.; Graham, D.; Smith, W. E. Comparison of Surface-Enhanced Resonance Raman Scattering and Fluorescence for Detection of a Labeled Antibody. *Anal. Chem.* **2008**, *80*, 2351–2356.
28. Feng, S.; Chen, R.; Lin, J.; Pan, J.; Chen, G.; Li, Y.; Cheng, M.; Huang, Z.; Chen, J.; Zeng, H. Nasopharyngeal Cancer Detection Based on Blood Plasma Surface-Enhanced Raman Spectroscopy and Multivariate Analysis. *Biosens. Bioelectron.* **2010**, *25*, 2414–2419.
29. Lin, J.; Chen, R.; Feng, S.; Pan, J.; Li, Y.; Chen, G.; Cheng, M.; Huang, Z.; Yu, Y.; Zeng, H. A Novel Blood Plasma Analysis Technique Combining Membrane Electrophoresis with Silver Nanoparticle-Based SERS Spectroscopy for Potential Applications in Noninvasive Cancer Detection. *Nanomedicine* **2011**, *7*, 655–663.
30. Lin, D.; Feng, S.; Pan, J.; Chen, Y.; Lin, J.; Chen, G.; Xie, S.; Zeng, H.; Chen, R. Colorectal Cancer Detection by Gold Nanoparticle Based Surface-Enhanced Raman Spectroscopy of Blood Serum and Statistical Analysis. *Opt. Express.* **2011**, *19*, 13565–13577.
31. Gracie, K.; Correa, E.; Mabbott, S.; Dougan, J. A.; Graham, D.; Goodacre, R.; Faulds, K. Simultaneous Detection and Quantification of Three Bacterial Meningitis Pathogens by SERS. *Chem. Sci.* **2014**, *5*, 1030–1040.
32. Prucek, R. R.; Ranc, V. V.; Kvítek, L. L.; Panáček, A. A.; Zbořil, R. R.; Kolář, M. M. Reproducible Discrimination between Gram-Positive and Gram-Negative Bacteria Using Surface Enhanced Raman Spectroscopy with Infrared Excitation. *Analyst* **2012**, *137*, 2866–2870.
33. Walter, A.; März, A.; Schumacher, W.; Rösch, P.; Popp, J. Towards a Fast, High Specific and Reliable Discrimination of Bacteria on Strain Level by Means of SERS in a Microfluidic Device. *Lab Chip* **2011**, *11*, 1013.
34. Nguyen, C. T.; Nguyen, J. T.; Rutledge, S.; Zhang, J.; Wang, C.; Walker, G. C. Detection of Chronic Lymphocytic Leukemia Cell Surface Markers Using Surface Enhanced Raman Scattering Gold Nanoparticles. *Cancer Lett.* **2010**, *292*, 91–97.
35. Jokerst, J. V.; Miao, Z.; Zavaleta, C.; Cheng, Z.; Gambhir, S. S. Affibody-Functionalized Gold-Silica Nanoparticles for Raman Molecular Imaging of the Epidermal Growth Factor Receptor. *Small* **2011**, *7*, 625–633.
36. Feng, S.; Lin, J.; Huang, Z.; Chen, G.; Chen, W.; Wang, Y.; Chen, R.; Zeng, H. Esophageal Cancer Detection Based on Tissue Surface-Enhanced Raman Spectroscopy and Multivariate Analysis. *Appl. Phys. Lett.* **2013**, *102*, 043702.
37. Sun, L.; Sung, K.-B.; Dentinger, C.; Lutz, B.; Nguyen, L.; Zhang, J.; Qin, H.; Yamakawa, M.; Cao, M.; Lu, Y.; *et al*. Composite Organic−Inorganic Nanoparticles as Raman Labels for Tissue Analysis. *Nano Lett.* **2007**, *7*, 351–356.
38. Lutz, B. R.; Dentinger, C. E.; Nguyen, L. N.; Sun, L.; Zhang, J.; Allen, A. N.; Chan, S.; Knudsen, B. S. Spectral Analysis of Multiplex Raman Probe Signatures. *ACS Nano* **2008**, *2*, 2306–2314.
39. Nolan, J. P.; Duggan, E.; Liu, E.; Condello, D.; Dave, I.; Stoner, S. A. Single Cell Analysis Using Surface Enhanced Raman Scattering (SERS) Tags. *Methods* **2012**, *57*, 272–279.
40. MacLaughlin, C. M.; Mullaithilaga, N.; Yang, G.; Ip, S. Y.; Wang, C.; Walker, G. C. Surface-Enhanced Raman Scattering Dye-Labeled Au Nanoparticles for Triplexed Detection of Leukemia and Lymphoma Cells and SERS Flow Cytometry. *Langmuir* **2013**, *29*, 1908–1919.
41. Wustholz, K. L.; Henry, A.-I.; McMahon, J. M.; Freeman, R. G.; Valley, N.; Piotti, M. E.; Natan, M. J.; Schatz, G. C.; Van Duyne, R. P. Structure−Activity Relationships in Gold Nanoparticle Dimers and Trimers for Surface-Enhanced Raman Spectroscopy. *J. Am. Chem. Soc.* **2010**, *132*, 10903–10910.
42. Moskovits, M. Persistent Misconceptions Regarding SERS. *Phys. Chem. Chem. Phys.* **2013**, *15*, 5301–5311.
43. Braun, G. B.; Lee, S. J.; Laurence, T.; Fera, N.; Fabris, L.; Bazan, G. C.; Moskovits, M.; Reich, N. O. Generalized Approach to SERS-Active Nanomaterials *via* Controlled Nanoparticle Linking, Polymer Encapsulation, and Small-Molecule Infusion. *J. Phys. Chem. C* **2009**, *113*, 13622–13629.
44. Guarrotxena, N.; Ren, Y.; Mikhailovsky, A. Raman Response of Dithiolated Nanoparticle Linkers. *Langmuir* **2011**, *27*, 347–351.
45. White, I. M.; Yazdi, S. H.; Yu, W. W. Optofluidic SERS: Synergizing Photonics and Microfluidics for Chemical and Biological Analysis. *Microfluid. Nanofluid.* **2012**, *13*, 205–216.

46. Xu, B.-B.; Ma, Z.-C.; Wang, H.; Liu, X.-Q.; Zhang, Y.-L.; Zhang, X.-L.; Zhang, R.; Jiang, H.-B.; Sun, H.-B. A SERS-Active Microfluidic Device with Tunable Surface Plasmon Resonances. *Electrophoresis* **2011**, *32*, 3378–3384.
47. Andreou, C.; Hoonejani, M. R.; Barmi, M. R.; Moskovits, M.; Meinhart, C. D. Rapid Detection of Drugs of Abuse in Saliva Using Surface Enhanced Raman Spectroscopy and Microfluidics. *ACS Nano* **2013**, *7*, 7157–7164.
48. Sha, M. Y.; Xu, H.; Natan, M. J.; Cromer, R. Surface-Enhanced Raman Scattering Tags for Rapid and Homogeneous Detection of Circulating Tumor Cells in the Presence of Human Whole Blood. *J. Am. Chem. Soc.* **2008**, *130*, 17214–17215.
49. Wang, X.; Qian, X.; Beitler, J. J.; Chen, Z. G.; Khuri, F. R.; Lewis, M. M.; Shin, H. J. C.; Nie, S.; Shin, D. M. Detection of Circulating Tumor Cells in Human Peripheral Blood Using Surface-Enhanced Raman Scattering Nanoparticles. *Cancer Res.* **2011**, *71*, 1526–1532.
50. Chang, H.-C.; Chen, T.-Y.; Hu, C.; Yang, F.-L. Rapid (<5 min) Identification of Pathogen in Human Blood by Electrokinetic Concentration and Surface-Enhanced Raman Spectroscopy. *Sci. Rep.* **2013**, *3*, 2365–2365.
51. Pallaoro, A.; Braun, G. B.; Moskovits, M. Quantitative Ratiometric Discrimination between Noncancerous and Cancerous Prostate Cells Based on Neuropilin-1 Overexpression. *Proc. Natl. Acad. Sci. U.S.A.* **2011**, *108*, 16559–16564.
52. Pallaoro, A.; Braun, G. B.; Reich, N. O.; Moskovits, M. Mapping Local pH in Live Cells Using Encapsulated Fluorescent SERS Nanotags. *Small* **2010**, *6*, 618–622.
53. Ellis, L. M. The Role of Neuropilins in Cancer. *Mol. Cancer Ther.* **2006**, *5*, 1099–1107.
54. Stiles, T.; Fallon, R.; Vestad, T.; Oakey, J.; Marr, D. W. M.; Squier, J.; Jimenez, R. Hydrodynamic Focusing for Vacuum-Pumped Microfluidics. *Microfluid. Nanofluid.* **2005**, *1*, 280–283.